The 3D nature of a real un-dismantled electrical contact interface

Roussos, Constantinos; Swingler, Jonathan

Published in:
Wear

DOI:
10.1016/j.wear.2015.01.078

Publication date:
2015

Wear 328-329 (2015) 115–122

Contents lists available at ScienceDirect

Wear

journal homepage: www.elsevier.com/locate/wear

The 3D nature of a real un-dismantled electrical contact interface

Constantinos Roussos *, Jonathan Swingler

School of Engineering and Physical Sciences, Heriot-Watt University, Edinburgh EH14 4AS, United Kingdom

ARTICLE INFO

Article history:
Received 17 October 2014
Received in revised form
24 January 2015
Accepted 28 January 2015
Available online 10 February 2015

Keywords:
Contacts
Contact area
Contact map
Contact resistance
X-ray CT

ABSTRACT

A 3D contact analysis and modeling suite of tools are developed and introduced in this work. The "3D Contact Map" of an electrical contact interface is presented demonstrating the 3D nature of the contact. It gives information on where the electrical contact spots in a 3D surface profile are located. An X-ray Computer Tomography (CT) technique is used to collect the 3D data to a resolution of around 5 μm of a real un-dismantled contact interface for analysis. Previous work by Lalechos and Swingler presented "2D Contact Map" on a 2D contact profile from collected 3D data to a resolution of around 8 μm. The main advantages of both 3D and 2D mapping techniques focus on the fact that they are non-destructive and there is no need to dismantle the component of interest. This current work focuses on the 3D mapping technique showing its advantages over the 2D mapping technique. For test purposes, a 16 A rated AC single pole switch is scanned after two different current loading tests (0 A and 16 A). A comparison for the total mechanical area of contact, the number of contact spots and the total contact resistance is conducted using both the 2D and 3D mapping techniques to a resolution of around 5 μm.

1. Introduction

Real surfaces contain peaks and valleys on the microscopic scale presenting a roughness. On this scale when two surfaces are brought together this roughness influences mechanical contact. It is evident that mechanical contact occurs only in a specific number of areas on the apparent area of contact. Surfaces have been discovered to have multi-scale characteristics with fractal behavior. As a result, there is great interest in surfaces and interfaces based on the representation of the surface as a fractal [1–7].

Various approaches have been used to understand contact phenomena. Initially, Holm [8] in the 1930s developed a fundamental theory to describe contact mechanisms and contact resistance. Over time, this theory has developed to include features such as asperity shape, contact spot number, contact spot distribution, material properties, surface profiles and operating conditions. Greenwood–Williamson's model [9], three decades after Holm's work, assumes that asperities on a surface are hemispherical in shape with the same radius. According to the Greenwood–Williamson model, the peaks of a surface of asperities are considered to be located at different heights following a random Gaussian distribution. The asperities undergo elastic deformation (considering the plastic deformation under particular conditions) when a Greenwood–Williamson surface comes into contact with a flat plane. This model has been further developed by many researchers including Majumdar and Bhushan [2] who create a fractal surface profile with different asperity radii.

Having more detailed knowledge of the physics and mechanisms of electrical contacts and their material properties helps in the design of devices with better performance and long-term reliability. This knowledge is beneficial for contact users, their suppliers and equipment system design engineers [10]. Various factors such as normal-force (applied force perpendicular to the surface), general contact design and electrical parameters have an impact on the reliability of contact systems [10]. The choice of normal-force and the general contact design are fundamental to a good contact so that an acceptable level for the operating life can be maintained. For example, the larger the area of contact is, the better the electrical contact in terms of lower contact resistance is.

Bowden and Tabor [11], introduced the plastic deformation relationship as shown in Eq. (1). Where A_p is the area of contact (under plastic deformation), F is the applied force and H is the hardness of the material.

$$A_p = \frac{F}{H} \tag{1}$$

Under elastic deformation of the materials, Hertz's contact theory [12,13] is used as shown in Eq. (2). Where A_e is the area of contact (under elastic deformation), F is the applied force, a is the radius of contacting spheres and E^* is a constant consisting of Young's modulus and Poisson's ratio of the materials involved.

$$A_e = \pi\left(\frac{3Fa}{4E^*}\right)^{2/3} \tag{2}$$

* Corresponding author. Tel.: +44 131 451 4148; fax: +44 131 451 4155.
E-mail address: cr83@hw.ac.uk (C. Roussos).

http://dx.doi.org/10.1016/j.wear.2015.01.078

According to Cooper et al. [14] the contact resistance can be calculated from the electrical contact spots each of which have independent constriction resistances which are all in parallel. For a single circular contact spot of radius α Holm [15] reported that the contact resistance R is given by Eq. (3). Where ρ, is the average value of the electrical resistivities for the two bodies in contact.

$$R = \frac{\rho}{2\alpha} \tag{3}$$

For a larger number of contact spots, assuming the electrical resistivity for the two bodies is constant, Eq. (3) for a distribution of such radius α_i, $i \in [1, n]$ (where i is the contact spot of interest and n is the total number of contact spots) can be written as follows:

$$R = \frac{\rho}{2\sum_{i=1}^{n} a_i} = \frac{\rho}{2n\overline{a}} \tag{4}$$

Where $\overline{\alpha}$ is the average value of a_i. According to Ciavarella et al. [16] commenting on the work of Jang and Barber [17], it is generally predicted by fractal contact theories that the $n\overline{\alpha}$ is unbounded with progressive scale refinement which leads to the unlikely conclusion that for a fractal surface the contact resistances due to surface roughness is always zero.

Greenwood in [18] reported that if a two scale structure consists of a set of n actual contact areas of radius α_i (first scale structure) clustered within a circular "contour area" of radius b (second scale structure), the contact resistance R is well approximated by the following

$$R = \frac{\rho}{2n\overline{a}} + \frac{\rho}{2b} \tag{5}$$

Moreover, Greenwood [18] derived a formula for the contact resistance which depends on the distances between the set of circular contact spots. The Greenwood formula of the contact resistance is given by Eq. (6). Where a_i is the radius of contact spot i, a_j the radius of contact spot j and d_{ij} is the distance between the contact spots i and j.

$$R = \rho\left(\frac{1}{2\sum a_i} + \frac{1}{\pi\left(\sum a_i\right)^2}\sum\sum_{i\neq j}\frac{a_i a_j}{d_{ij}}\right) \tag{6}$$

In this current work, the Greenwood formula (Eq. (6)) is used to calculate the contact resistance from real data acquired using an X-ray CT visualization technique to a resolution of around 5 μm. The X-ray CT visualization technique was used previously by Lalechos and Swingler [19,20] to a resolution of around 8 μm. They pictured an actual contact interface as a "2D Contact Map" presenting the contact interface as a 2D surface plane. The current work shows the contact interface is not a 2D surface plane between contacting bodies but a 3D surface profile. Some initial work has been presented by the authors which shows the evaluation of electrical contacts using an X-ray CT visualization technique [21]. This current work presents the actual contact interface in a "3D Contact Map" compared with the "2D Contact Map" for 0 A and 16 A AC. A suite of tools of Contact Analysis Techniques (CAT*) are developed to achieve this.

2. Visualization techniques

The internal features of a contact interface object can be visualized using different methods. Visualization techniques can be categorized into destructive and non-destructive. Destructive techniques involving Thermo-Graphic (TG) [22] and Scanning Electron Microscopy (SEM) [23,24] can be applied if one part of the interface is substituted to enable the viewing of the interface. If both parts of the original contact are to be investigated, then dismantling for analysis results in many of the features of interesting being destroyed (more examples for destructive techniques are given in reference [21]). More studies in recent times are focused on non-destructive techniques involving Magnetic Resonance Imaging (MRI) and X-ray CT. These offer the possibility to acquire 2D and 3D views of samples without dismantling the component parts and thus not destroying any features of interest.

Zhu et al. [25] used MRI to show the effectiveness of this technique for the visualization of transparent and non-transparent components measuring the internal contact angles between solids and liquids. A drawback of the MRI technique is that the sample should not include ferrous materials (Fe, Ni and Co) because of interaction with the applied high magnetic fields.

Johnson et al. [26] have also used the MRI technique to visualize the radio-lunate and radio-scaphoid joints within a human body. The acquired images of the technique were used to create model geometry and kinematics for the calculation of peak contact pressures and average contact pressures, contact forces and contact areas.

The X-ray CT technique has been used much more than the MRI technique in engineering and analysis of samples such as by Popovich et al. [27] and Green et al. [28]. Popovich et al. [27] used it to characterize the internal microstructure in multi-crystalline silicon solar cells. Green et al. [28] used the technique to calculate the contact area of gas/liquid and liquid "holdup" in structured packing.

Moreover, Lalechos and Swingler [20] used the X-ray CT technique to identify the contact spots which are in mechanical contact without dismantling the specimens and produced "2D Contact Map" of portion of areas of the electrical contact interface. From the contact maps much information can be extracted such as the area and the number of contact spots, the distance between them and the total contact resistance using appropriate models [19,20,29]. In this current work, a comparison for the total mechanical area of contact, the number of contact spots and the total contact resistance is conducted using both the 2D and 3D mapping techniques to a resolution of around 5 μm.

3. Experimental methodology

3.1. Acquiring 3D X-ray CT data

The X-ray CT used in this work consists of the X-ray source, the rotary turntable and a 2D pixel array detector. The X-ray source operates at 175 kV and 133 μA. The sample is placed on the rotary turntable which enables the acquisition by the detector of 2439 2D X-ray images as the sample is rotated 360°. The reconstruction of the 2D X-ray images into the 3D model of the sample is achieved with CT-Pro software. After this process, VGStudioMax software is used to create 2D cross-sectional slice images from the 3D model.

The procedure used to obtain the reconstruction of the 3D model and 2D cross-sectional slice images is shown in Fig. 1. Firstly, the sample is illuminated with the X-rays from the source and the detector records the 2D X-ray image. Every time the turntable is rotated by $\sim 0.15^{\circ}$, a 2D X-ray image is acquired until the turntable has been rotated by 360°. The level of X-ray intensity across an x–y plane is recorded as the 2D X-ray image. This relates to the level of admittance of the X-ray along the z-direction through the whole sample for the x–y plane. Each of the 2D X-ray images consists of information regarding the X-ray admittance character of the materials through the whole sample. The CT-Pro software uses the 2D X-ray images to reconstruct them into a 3D model. From this, a series of x–y 2D cross-sectional slice images across the sample can be obtained in the z-direction through the sample.

3.2. A suite of Contact Analysis Techniques (CAT*) tools

For the analysis of the 2D cross-sectional slice images and 3D reconstruction models, Contact Analysis Techniques, or CAT* are developed and implemented with a suite of tools developed using

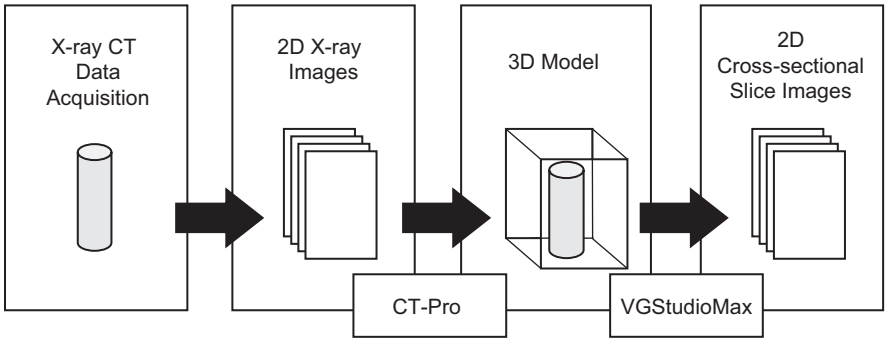

Fig. 1. Data acquisition.

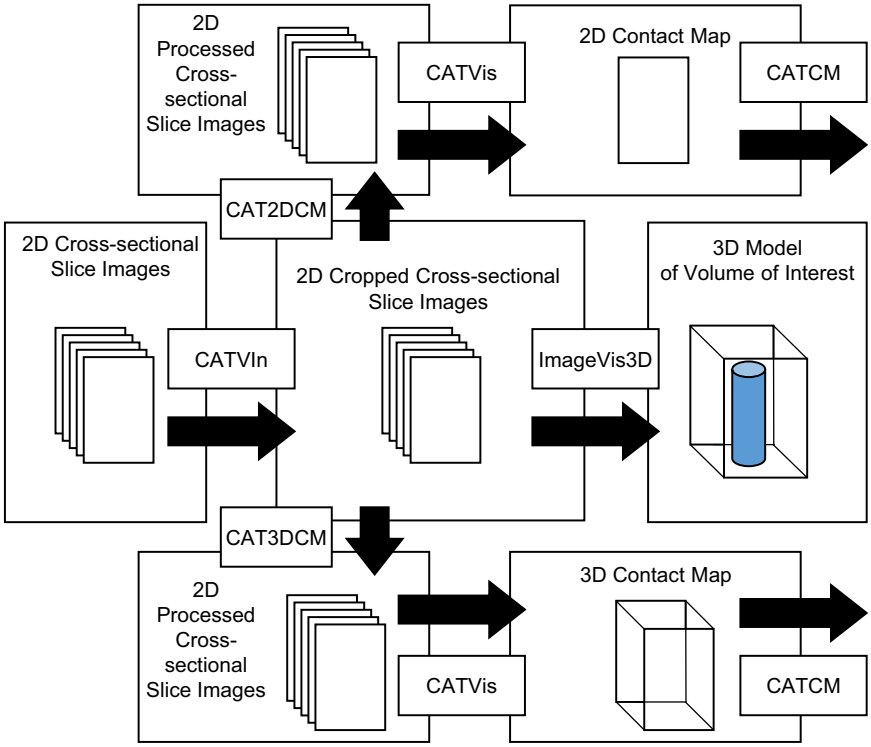

Fig. 2. Analysis tools diagram.

Matlab and Image Processing Toolbox. The different tools are shown in Fig. 2.

Initially, Contact Analysis Technique for Volume of Interest (CATVIn) analysis tool is used to process the 2D cross-sectional slice images cropping the areas of interest. For the visualization of the volume of interest, ImageVis3D software is used.

Contact Analysis Technique for 2D Contact Map (CAT2DCM) and Contact Analysis Technique for 3D Contact Map (CAT3DCM) analysis tools are used for the development of 2D and 3D contact maps respectively using the 2D cropped cross-sectional slice images which are produced from the CATVIn analysis tool. For the visualization of both 2D and 3D contact maps Contact Analysis Technique for Visualization (CATVis) is used. Moreover, for both 2D and 3D contact maps Contact Analysis Technique for Contact Map (CATCM) analysis tool is used for the calculation of the total mechanical area of contact, the number of contact spots and the total contact resistance.

3.3. 2D cross-sectional slice images information

Fig. 3 shows a 2D cropped cross-sectional slice image of the Conductors 1 and 2 of the contact pair which are in mechanical contact across the interface of interest. The resolution of the 2D cross-sectional slice image in this study is found to be $4.95 \pm 0.05\ \mu m$ for pixel length. The resolution is found by measuring the actual length between particular characteristics in the sample (e.g. length of a conductor) with a standard micro-meter and pinpointing these characteristics in the data set. These 2D cropped cross-sectional slice images are used in the ImageVis3D software and CAT* suite of tool for analysis. A detailed explanation of the techniques used in the CAT* suite of tools is given in Section 4.

3.4. Sample under investigation and macro-visualization

A single pole rocker switch rated at 16 A AC with dimensions $(3.0 \times 2.5 \times 3.5)$cm is used as a sample for the investigation. The contact material is made of a silver alloy and other conductors are made from a copper alloy. The internal view of the metalwork of the single pole rocker switch is shown in Fig. 4a. It consists of conductors and contact force spring. The geometry of the contact pair is a flat on flat with surface roughness, $R_a = 0.32\ \mu m$. The surface roughness test was carried out using a contact profilometer Taylor-Hobson RTH Talysurf 5–120 with a lateral x resolution of

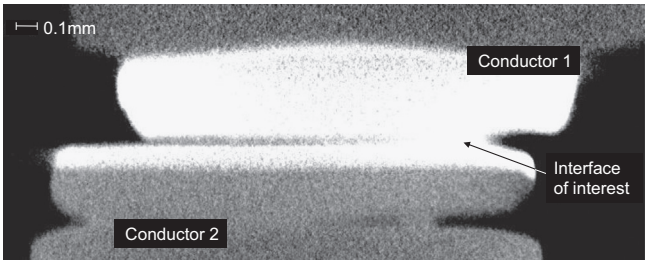

Fig. 3. 2D cross-sectional slice image of a single pole switch.

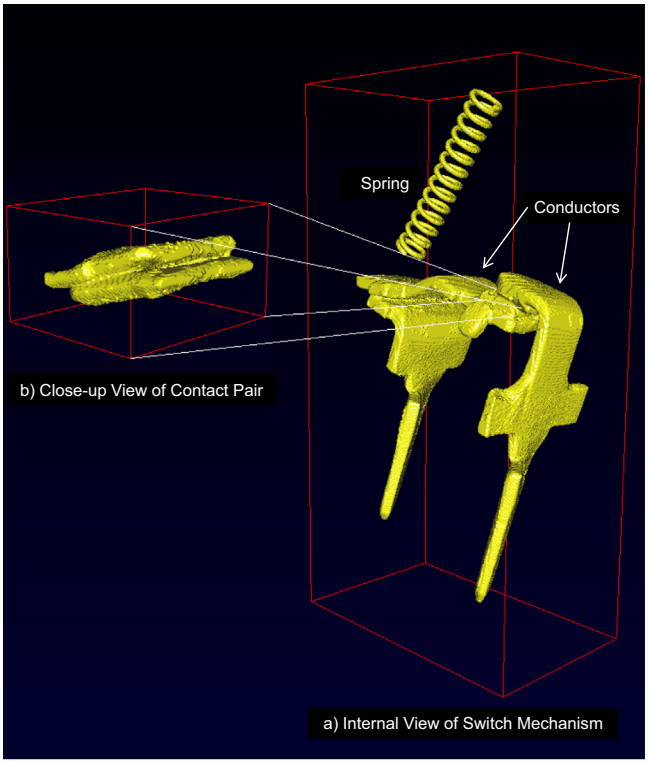

Fig. 4. Microscopic 3D model of internal view of switch mechanism.

0.1 μ*m* and height *z* resolution of 0.1 nm. The contact force is found to be $F = 1.89 \pm 0.07$ N and the electrical resistance across the contact pair, R_{cp} was found using the "four-wire" method to be $\sim 0.27\ m\Omega$.

Fig. 4b shows the close-up view of a closed contact pair of the single pole rocker switch which is the volume of interest. For the 3D visualization of the close-up view of a closed contact pair CATVIn analysis tool and ImageVis3D software are used as described in Fig. 2.

4. Contact analysis and modeling techniques

Cross-sectional slice images of the contact interface are used to produce 2D and 3D contact maps. 2D contact maps (as produced by Swingler and Lalechos [19,20]) can be significantly different to 3D contact maps under particular conditions which will be discussed in Section 6. Fig. 5 illustrates how both techniques work for a simple case. Fig. 5a shows the schematic cross-sectional slice image of Bodies 1 and 2 which are in mechanical contact. The white areas of the schematic cross-sectional slice image between the two bodies are indicating voids and open spaces.

Fig. 5b shows the result of the 2D contact mapping technique of the schematic cross-sectional slice image of Fig. 5a, where the

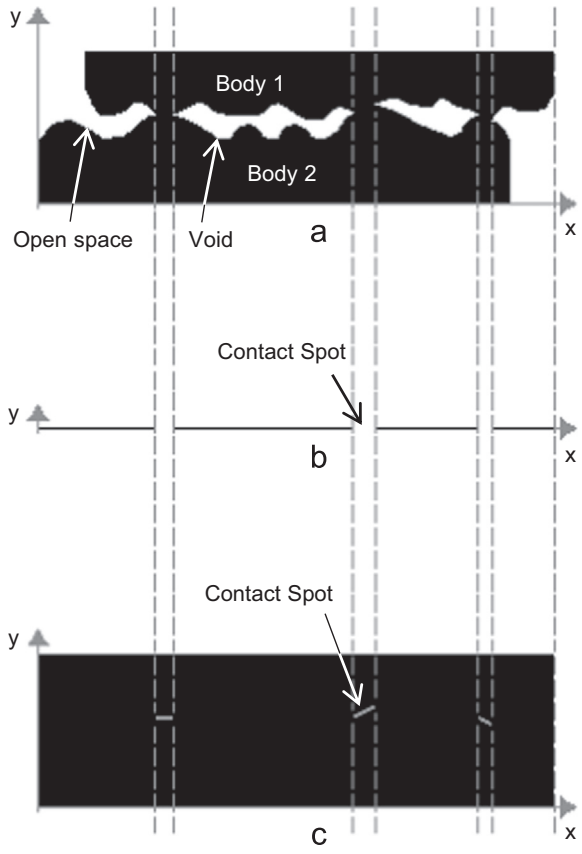

Fig. 5. Schematic cross-section slice of (a) Bodies 1 and 2 in mechanical contact, (b) 2D contact mapping technique, and (c) 3D contact mapping technique.

white areas (on the *x*-axis) in this case are illustrated to be in mechanical contact. The height of contact spots on the *y*-axis in the 2D contact maps is lost (*y*-direction is equal with zero). This type of technique was used by Lalechos and Swingler [19,20] and puts the contact interface onto a 2D plane when all cross-sectional slice images are joined together.

Fig. 5c shows the result of the 3D contact mapping technique of the schematic cross-sectional slice image in Fig. 5a. This is a new technique for the visualization of the contact interface in the 3D plane developed in this work. The white areas of Fig. 5c are indicating mechanical contact spots. In this technique, the contact spots are the line segments which are connecting the voids (and open spaces). The contact interface forms a 3D profile when all cross-sectional slice images are joined together.

The 3D contact mapping technique uses a 3D reconstruction model of the data taken from the cross-sectional slice images. A further technique is used to identify the contact spots and gives information on their 3D position. This technique consists of three steps. Firstly, it is required to divide the sample into equal cross-sectional slices across one of the three directions. Secondly, the direction of the normal force (F) is identified and in this work is defined to be perpendicular to one of the other two directions. The direction of the normal force is used to define the orientation of the coordinate system used. The last step is the examination of each cross-sectional slice separately to generate the final result.

For example, Fig. 6 shows a schematic close-up of a cross-sectional slice of a sample which is divided in equal slices in the *z*-direction and the normal force is perpendicular to the x-direction (or parallel with *y*-direction). The sample consists of two bodies (Body 1 and Body 2) which are in contact (at points across the line segment *AB*) having two voids where their circumferences are described by different functions ($f_n(x,y)$ and $f_{n+1}(x,y)$).

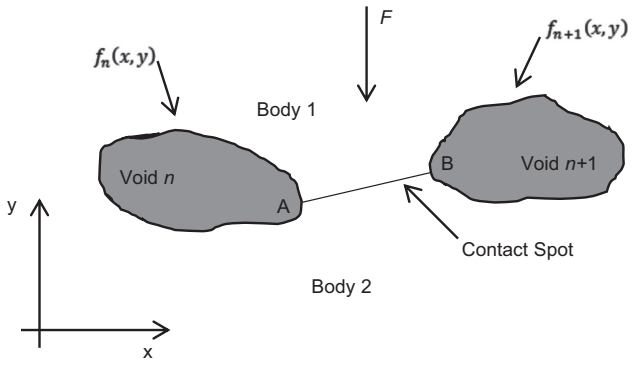

Fig. 6. Schematic cross-section slice of a contact spot.

From Fig. 5a it is obvious that the contact spots are presented between the voids which are the result of the roughness of the two bodies. Eq. (7) describes the line segment (contact spot) *AB* which is the connection of the maximum value x of void n (x_{max_n}) with the minimum value of x of void $n+1$ ($x_{min_{n+1}}$).

$$f_{zl}(x) = \frac{f_{n+1}(x_{min_{n+1}}) - f_n(x_{max_n})}{x_{min_{n+1}} - x_{max_n}}(x - x_{max_n}) + f_n(x_{max_n}) \quad (7)$$

The coordinates of the points A and B are $(x_{max_n}, f_n(x_{max_n}))$ and $(x_{min_{n+1}}, f_{n+1}(x_{min_{n+1}}))$ respectively, because the x values of points A and B belong to the voids, $x \in (x_{max_n}, x_{min_{n+1}})$. The suffix z in Eq. (7) is the number of the cross-sectional slice, $z \in [1, i]$ (i is the total number of cross-sectional slices). The suffix l is the number of the contact spot in each cross-sectional slice, $l \in [n-1, n]$ with $n \in [2, \kappa]$. Where n is the number of void (or open space) and κ is the total number of voids in each cross-sectional slice ($\kappa \geq 2$ because each cross-sectional slice has 2 open spaces, which are consider as voids across the x-direction). The 3D contact map consists of the plot of all line segments for all cross-sectional slices in 3D plane.

In this work, a contact spot is defined as a collection of contacting pixels which are neighboring other contacting pixels by at least one of their sides. Fig. 7 shows a plan view of 3 contact spots. Contact Spot 1 consists of 5 contacting pixels, Contact Spot 2 consists of 29 contacting pixels and Contact Spot 3 consists of only 1 contacting pixel. It is important to mention that a contacting pixel which is only diagonal with a neighbor contacting pixel belonging to a contact spot is not considered to be a part of that spot (see Contact Spots 2 and 3 of Fig. 7). The mean-point pixel is the point with the mean values of x and z (and y in 3-axes) of each contact spot.

Eq. (6) is used to calculate the contact resistance. To achieve this, each contact spot is assumed to be a circle of radius a. For example, the radius of contact spot i is calculated from the following equation:

$$a_i = \sqrt{\frac{A_i}{\pi}} \quad (8)$$

where A_i is the total contact area of contact spot i. The distance between contact spot i and j is calculated from the mean-points of the contact spots i and j.

5. Results and analysis

5.1. 2D contact maps

Fig. 8 shows two microscopic 2D contact maps of the contacting interface of the contact pair (conductors 1 and 2) within the switch sample. The white areas illustrate mechanical contact consisting of "contacting" pixels. The switch sample was scanned twice with the X-ray CT. The first scan was held after non-current loading and the second one was held approximately thirty days after being stored in the lab and loaded with current at 16 A AC for 48 h. Fig. 8a is the 2D contact map from the first scan at 0 A and Fig. 8b is from the second scan at 16 A.

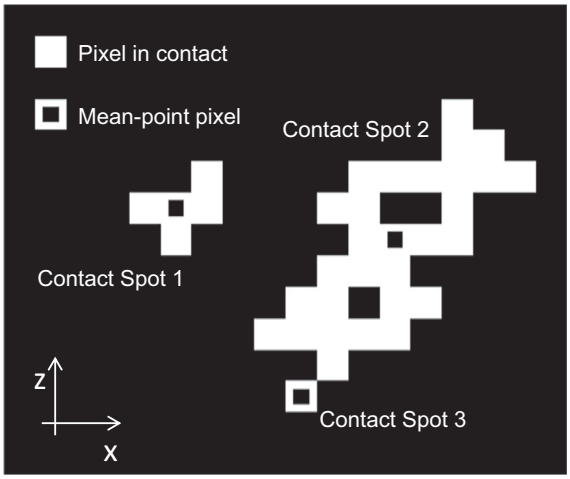

Fig. 7. Contact spots.

For the analysis of 2D contact maps the CATCM analysis tool is used for the calculation of the total mechanical area of contact A_T, the number of contact spots n_s and the contact resistance R (Eq. (6) was used with $\rho = 15.87 \times 10^{-9}$ Ωm, electrical resistivity of silver at 20 °C). The results for both 2D contact maps are presented in Table 1. The 2D contact map at 0 A has 592 contact spots with total mechanical area of contact 1.85 ± 0.03 mm^2 and contact resistance 2.16 ± 0.02 μΩ. At 16 A 2D contact map, the number of contact spots and the total mechanical area of contact are decreased to 259 and 1.55 ± 0.03 mm^2 respectively while the contact resistance is increased to 4.27 ± 0.04 μΩ.

5.2. 3D contact maps

Fig. 9 shows the microscopic 3D contact maps of the contacting interface of the switch sample for the two different scans at 0 A and 16 A as used in the 2D analysis.

The CATCM analysis tool is also used for 3D contact analysis for the calculation of the total mechanical area of contact A_T, the number of contact spots n_s and the contact resistance R. The results for both 0 A and 16 A 3D contact maps are presented on Table 2. The 3D contact map at 0 A has 610 contact spots with total mechanical area of contact 1.86 ± 0.03 mm^2 and contact resistance of 2.07 ± 0.02 μΩ. At 16 A 3D contact map, the number of contact spots and the total mechanical area of contact are decreased to 247 and 1.56 ± 0.03 mm^2 respectively unlike with the value of contact resistance which is increased to 4.42 ± 0.04 μΩ.

6. Discussion

6.1. The X-ray CT technique

The results show that the X-ray CT technique is a useful tool for viewing the contact interface without dismantling the sample and determining the total mechanical area of contact, the number of contact spots and the contact resistance. The images obtained with the current facility give a pixel resolution of 4.95 $\mu m \times 4.95$ μm and an area resolution of 24.5 μm^2 which is $5\frac{1}{2}$ and $1\frac{3}{5}$ times higher in resolution than previous work [21] and Swingler work [29,30] on different facilities respectively.

Resolution is an important factor for the visualization and calculation techniques. For example, for a coarse measurement (e.g 100 μm)

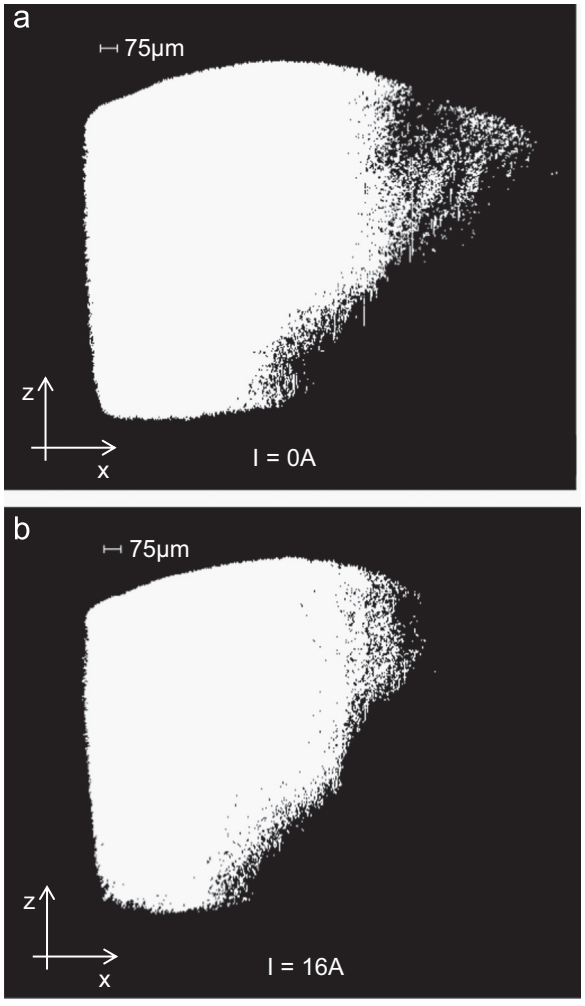

Fig. 8. Microscopic 2D contact maps.

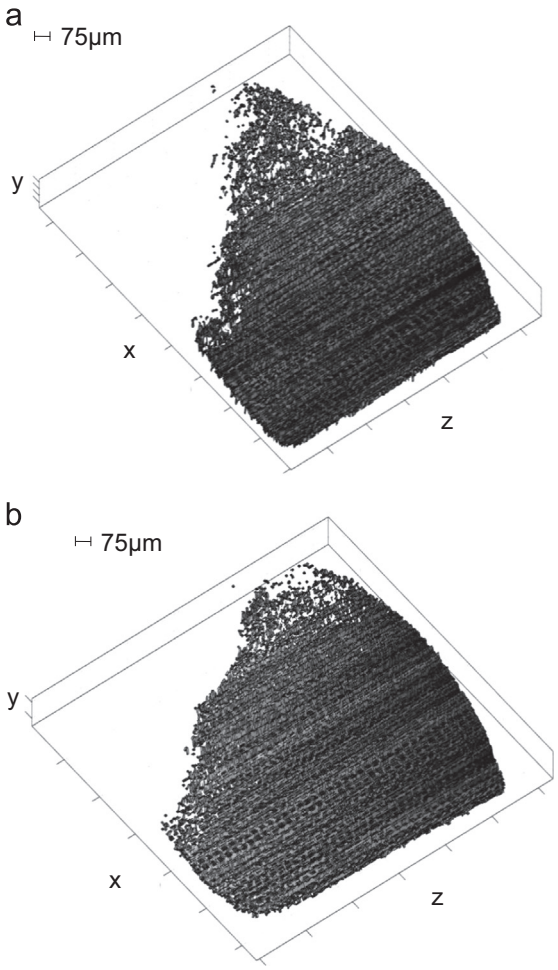

Fig. 9. Microscopic 3D contact maps.

Table 1
2D Contact maps characteristics.

I (A)	n_s	A_T (mm^2)	R (μΩ)
0	592	1.85 ± 0.03	2.16 ± 0.02
16	259	1.55 ± 0.03	4.27 ± 0.04

Table 2
3D Contact maps characteristics.

I (A)	n_s	A_T (mm^2)	R (μΩ)
0	610	1.86 ± 0.03	2.07 ± 0.02
16	247	1.56 ± 0.03	4.42 ± 0.04

of resolution, only a few asperities of large curvature are visualized while for smaller measurement (e.g 0.1 μm) of resolution, more asperities of smaller curvature are visualized [16,30]. The smallest resolution which can be obtained by the current facility is 3 μm. This depends on the sample dimensions and X-ray admittance of the sample materials. The resolution of 4.95 ± 0.05 μm obtained in this work is the optimum that could be achieved with the sample configuration used. Ideally, a resolution in the order of 0.1 μm is needed to investigate a Greenwood–Williamson model of the asperities. However, it should be noted that the Contact Analysis Techniques (CAT*) developed and implemented within a suite of tools in this work can be used with data of finer resolution. Nonetheless, some interesting features have been found with the data obtained which are discussed below.

6.2. 2D and 3D contact mapping techniques

Analysis and modeling techniques are developed to produce 3D contact maps of an electrical contact interface which for the first time gives information as to where the electrical contacts in a 3D volume are located to a microscopic resolution. The mathematical modeling at the contact spots is described by Eq. (7). The equation describes a line segment or a series of line segments through each contact spot and every contact spot at the interface.

Contact maps are visualized for different electric current values in 2D (Fig. 8) and 3D (Fig. 9). The electric current values chosen (0 A and 16 A AC) represent the low and high current limits of the example switch sample chosen (rated at 16 A AC). The analysis of the contact map data (Table 1 from 2D mapping technique and Table 2 from 3D mapping technique) shows that the number of contact spots and the total mechanical area of contact are smaller at the higher current irrespective of whether using the 2D mapping technique or the 3D mapping technique. The contact resistance, thus, is higher after the sample has been stressed with the 16 A current loading. This is indicating that current stressing a contact pair reduces the number of smaller spots and the dispersion of those spots. This may be due to local heating and melting at the contact spots causing them to come together. These are only initial results as more samples need to be investigated.

6.3. Loss of information with 2D contact maps

Comparing the 2D mapping technique with the 3D mapping technique shows some points that need to be noted since data in Table 1 and data in Table 2 are different. At 0 A the number of contact spots produced by the 2D mapping technique is 592 whereas when using the 3D mapping technique this has increased to 610. At 16 A the number of contact spots produced by the 2D mapping technique is 259 whereas using the 3D mapping technique this has decreased to 247. This difference is a result of two issues which the 2D contact mapping technique presents. These are explained below.

The first issue, given the label of "Neighboring Contact Spot Aggregation Error", is where multiple neighboring contact spots as visualized in 3D are seen as one contact spot in 2D visualizations. This is a result of the contact interface in reality being a 3D surface and when analyzed with the 2D mapping technique the height (y-direction) information of that x–z surface is omitted from the data. The explanation of this issue is illustrated in Fig. 10. Fig. 10a shows the 2D contact mapping technique of a single contact spot which is developed by 2 cross-sectional slice images and consists of 8 contacting pixels. The single contact spot shown in Fig. 10a is presented in Fig. 10b in 3D contact mapping technique as 4 contact spots. For the definition of contact spot in 3D contact maps, a technique used in 2D contact maps is used as well. A contact spot in 3D contact map is defined as a collection of contacting voxels ("3D pixels") which are neighboring other contacting voxels with at least one of their sides. Contact Spot 1 in Fig. 10b consists of only 1 contacting voxel, Contact Spot 2 consists of 2 contacting voxels, Contact Spot 3 consists of 2 contacting voxels and Contact Spot 4 consists of 3 contacting voxels. Due to the "Neighboring Contact Spot Aggregation Error" of the 2D mapping technique, this results in less small contact spots but same total mechanical area of contact compared to the 3D mapping technique.

The second issue, given the label of "Overlapping Void Disaggregation Error", is where overlapping voids in the y-directions (and

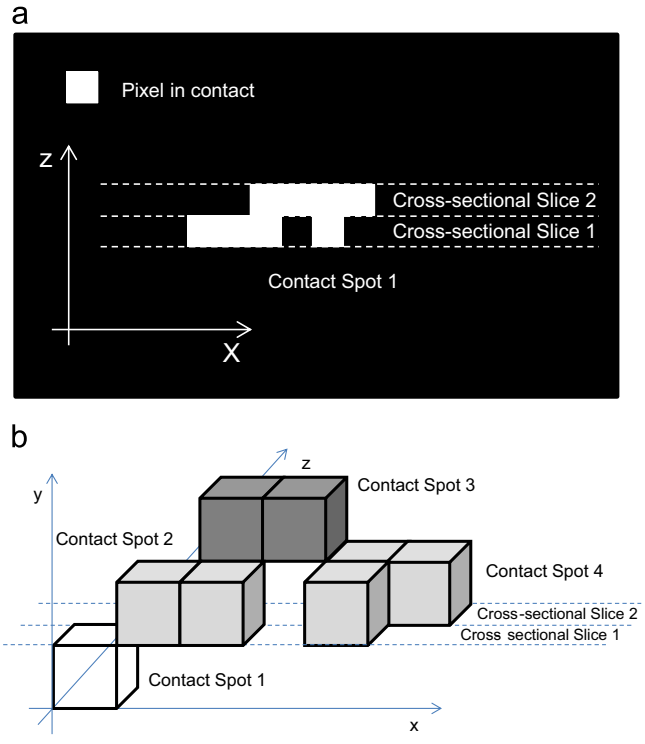

Fig. 10. Contact spots in 2D and 3D contact maps.

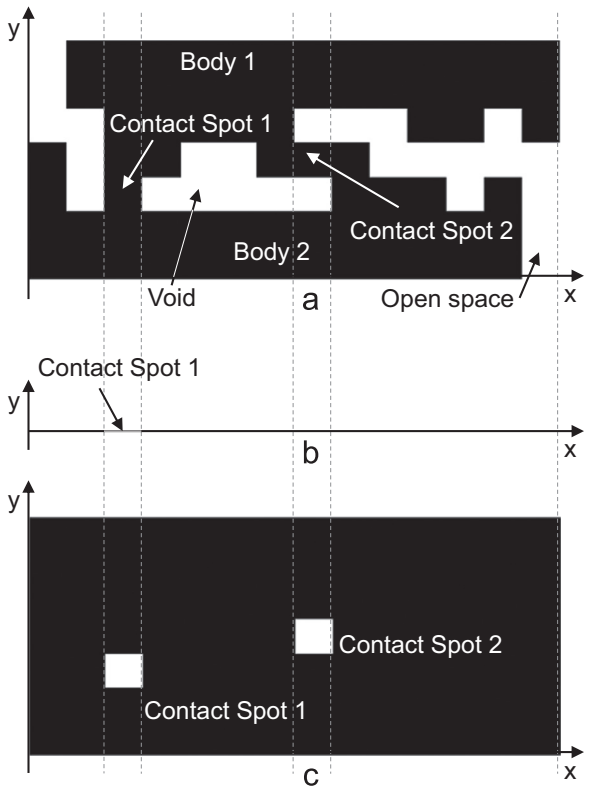

Fig. 11. Peak and side contact spots. Schematic cross-section slice of (a) Bodies 1 and 2, (b) 2D contact mapping technique, and (c) 3D contact mapping technique.

associated multiple spots visualize in 3D) mask contact spots when seen in 2D visualizations. This again is a result of the contact interface in reality being a 3D surface and when analyzed with the 2D mapping technique the height (y-direction) information of that x–z surface is omitted from the data. The explanation of this issue is illustrated in Fig. 11. Fig. 11a shows the schematic cross-sectional slice image of Bodies 1 and 2 which are coming in mechanical contact. The white areas of the schematic cross-sectional slice image between the two bodies are indicating voids and open spaces. Where Contact Spot 1 is the mechanical contact created by the top surfaces at the peaks of two bodies and Contact Spot 2 is the mechanical contact created by portions of side surfaces of the peaks of two bodies. Fig. 11b shows the 2D contact mapping technique which illustrates only the Contact Spot 1. The 3D contact mapping technique in Fig. 11c in contrast to Fig. 11b illustrates all the contact spots (Contact Spot 1 and Contact Spot 2). Due to the "Overlapping Void Disaggregation Error" of the 2D mapping technique, this results in less contact spots and also smaller total mechanical area of contact compared to the 3D mapping technique.

6.4. Area of contact findings

The total mechanical area of contact for the 0 A case is found to be 1.85 ± 0.03 mm^2 by using the 2D contact mapping technique which is within the error limits of 1.86 ± 0.03 mm^2 when using the 3D contact mapping technique. Again for the total mechanical area of contact for the 16 A case is found to be 1.55 ± 0.03 mm^2 by using the 2D contact mapping technique is within the error limits of 2.56 ± 0.03 mm^2 when using the 3D contact mapping technique. Comparing the corresponding values of the total mechanical area of contact in Tables 1 and 2 it is obvious that they are very close with difference value equal with 0.01 mm^2. At this point, it is important to mention that Lalechos et al. [19] reported that the result of the calculation of the total mechanical area of contact using 2D contact

mapping technique gives values close to experimental findings using Bowden and Tabor [11] formula (Eq. (1)).

6.5. Contact resistance findings

The contact resistance for the 0 A case by using the 2D contact mapping technique is $2.16 \pm 0.02\ \mu\Omega$ which decreases to $2.07 \pm 0.02\ \mu\Omega$ when using the 3D contact mapping technique. The contact resistance for the 16 A case by using the 2D contact mapping technique is $4.27 \pm 0.04\ \mu\Omega$ which increases to $4.42 \pm 0.04\ \mu\Omega$ when using the 3D contact mapping technique. The difference in corresponding values in 2D and 3D contact maps is a result of the two issues analyzed beforehand in this section. According to Greenwood [18] the contact resistance (Eq. (6)) depends on the number of contact spots, the radius of each contact spot and the distances between them. The contact resistance found form the mapping techniques is much lower than values measured across the contact pair $(R_{cp} \approx 0.27\ m\Omega)$. It is thought that the measurement is much larger because an ideal four-wire technique is not possible for the sample and bulk material is still measured as well as the constrictions resistance of the spots.

7. Conclusion

The X-Ray CT technique has been used to produce 2D and 3D contact maps of a 16 A AC single pole switch interfaces without the need to dismantle the sample. The sample was investigated before and after current loading of 16 A. For the 2D and 3D contact maps, Contact Analysis Techniques, CAT*, are developed and implemented with a suite of tools developed in Matlab which can be used for any value of resolution. It is found that the total mechanical area of contact and number of contact spots decrease after current loading whether using the 2D or 3D contact mapping technique. Thus, the contact resistance is found to increase after current loading. However, it is found that the different techniques (2D or 3D) produced different results. The 3D mapping technique demonstrates that the contact interface is not a 2D plane but has a 3D nature. This is important when analysing contact interfaces. The 2D mapping technique is shown to have issues with “Neighboring Contact Spot Aggregation” and the “Overlapping Void Disaggregation” as information in the third dimension can be lost due to the 3D nature of a contacting surface interface. Thus, a 3D analysis technique should be used when investigating contact interfaces.

Acknowledgments

This work is supported by a DTA studentship funded by U.K. Engineering and Physical Sciences Research Council (EPSRC). Aspects of this work are made possible in part by the use of the ImageVis3D software owned by Utah.edu which was funded by the NIH/NCRR Center for Integrative Biomedical Computing, P41-RR12553 and the DOE SciDAC Visualization and Analytics Center for Enabling Technologies, DEFC0206ER25781.

References

[1] A. Majumdar, B. Bhushan, Fractal model of elastic–plastic contact between rough surfaces, J. Tribol. 113 (1991) 11–22.
[2] B. Bhushan, A. Majumdar, Characterization and modeling of surface roughness and contact mechanics, Handbook of Micro/Nano Tribology, CRC Press, New York (1995) 109–165.
[3] F.M. Borodich, A.B. Mosolov, Fractal roughness in contact problems, J. Appl. Math. Mech. 56 (1992) 681–690.
[4] F.M. Borodich, D.A. Onishchenko, Similarity and fractality in the modelling of roughness by a multilevel profile with hierarchical structure, Int. J. Solids Struct. 36 (1999) 2585–2612.
[5] J. Lopez, G. Hansal, J.C.L. Bossé, T. Mathia, Caractérisation fractale de la rugosité tridimensionnelle d'une surface, J. Phys. III 4 (1994) (2501-2219).
[6] K.L. Johnson, Contact Mechanics, Cambridge University Press, Cambridge (1985) 407.
[7] G. Palasantzas, J.T.M.D. Hosson, Self-affine roughness effects on the contact area between elastic bodies, J. Appl. Phys. 93 (2003) 898–902.
[8] W. Shujuan, H. Fang, S. Bonan, Z. Guofu, Method for calculation of contact resistance and finite element simulation of contact temperature rise based on rough surface contact model, in: Proceedings of the 26th International Conference on Electrical Contacts (ICEC 2012), Beijing, China, May 2012, pp. 317–321.
[9] J.A. Greenwood, J.B.P. Williamson, Contact of nominally flat surfaces, Proc. R. Soc. Lond. Ser. A Math. Phys. Sci. 295 (1966) 300–319.
[10] P.V. Dijk, Critical aspects of electrical connector contacts, in: Proceedings of the 2nd International Conference on Reliability of Electrical Products and Electrical Contacts (ICREPEC 2007), Xiamen, China, 2007.
[11] F.P. Bowden, D. Tabor, Area of contact between solids, The Friction and Lubrication of Solids, Clarendon Press, Oxford, 2001.
[12] R. Holm, Theory and Applications Electric Contacts, Springer, Berlin, 1967.
[13] R.D. Mindlin, Compliance of elastic bodies in contact, J. Appl. Mech. 16 (1949) 259–268.
[14] M. Cooper, B. Mikic, M. Yovanovich, Thermal contact conductance, Int. J. Heat Mass Transf. 12 (1969) 279–300.
[15] R. Holm, Electric Contacts Handbook, third ed., Springer Verlag, Berlin, 1958.
[16] M. Ciavarella, G. Demelio, J.R. Barber, Y.H. Jang, Linear elastic contact of the Weierstrass profile, Proc. R. Soc. Lond. Ser. A 456 (2000) 387–405.
[17] J.R. Barber, Bounds on the electrical resistance between contacting elastic rough bodies, Proc. R. Soc. Lond. Ser. A 459 (2003) 53–66.
[18] J.A. Greenwood, Constriction resistance and the real area of contact, J. Appl. Phys. 17 (1966) 1621–1632.
[19] A.V. Lalechos, J. Swingler, J.W. McBride, Evaluation of the X-ray CT visualisation technique for characterising electrical contacts, in: Proceedings of the 56th IEEE Holm Conference on Electrical Contacts, Charleston, SC, October 2010, pp. 1–6.
[20] A.V. Lalechos, J. Swingler, J. Crane, Visualisation of the contact area for different contact forces using X-ray computer tomography, in: Proceedings of the 54th IEEE Holm Conference on Electrical Contacts, Orlando, FL, October 2008, pp. 263–269.
[21] C. Roussos, J. Swingler, Evaluation of electrical contacts using an X-ray CT 3D visualisation technique, in: Proceedings of the 27th International Conference on Electrical Contacts (ICEC 2014), Dresden, Germany, June 2014, pp. 326–331.
[22] M. Myers, M. Leidner, H. Schmidt, Effect of contact parameters on current density distribution in a contact interface, in: Proceedings of the 57th IEEE Holm Conference on Electrical Contacts, Minneapolis, MN, September 2011, pp. 1–9.
[23] M. Braunovic, N.K. Myshkin, V.V. Konchits, Fundamentals, Applications and Technology, Electrical Contacts, CRC Press, New York, 2007.
[24] J. Goldstein, D.E. Newbury, D.C. Joy, C.E. Lyman, P. Echlin, E. Lifshin, L. Sawyer J.R. Michael, Scanning Electron Microscopy and X-ray Microanalysis, third ed., Springer, New York, 2003.
[25] W. Zhu, Y. Tian, X. Gao, L. Jiang, A method to measure internal contact angle in opaque systems by magnetic resonance imaging, ACS J. Surf. Colloids 29 (2013) 9057–9062.
[26] J.E. Johnson, T.E. Mclffb, P. Leec, E.B. Tobyb, K.J. Fischera, Validation of radiocarpal joint contact models based on images from a clinical MRI scanner, Comput. Methods Biomech. Biomed. Eng. 17 (2014) 378–387.
[27] V.A. Popovich, W. Verwaal, M. Janssen, I.J. Bennett, I.M. Richardson, Application of X-ray computed tomography in silicon solar cells, in: Proceedings of the 35th IEEE Photovoltaic Specialists Conference (PVSC), Honolulu, HI, June 2010, pp. 1759–1764.
[28] C.W. Green, J. Farone, J.K. Briley, R.B. Eldridge, R.A. Ketcham, B. Nightingale, Novel application of X-ray computed tomography: determination of gas/liquid contact area and liquid holdup in structured packing, Ind. Eng. Chem. Res. 46 (2007) 5734–5753.
[29] J. Swingler, A. Lalechos, Visualization and size distribution of contact spots at a real un-dismantled electrical contact interface, J. Phys. D: Appl. Phys. 42 (2009) 1–7.
[30] J. Swingler, The resolution dependence of measured fractal characteristics for a real un-dismantled electrical contact interface, Wear 268 (2010) 1178–1183.